

Benchmark Study of Alkane Molecular Chains

Van Veen, Frederik H.; Ornago, Luca; Van Der Zant, Herre S.J.; El Abbassi, Maria

DOI

[10.1021/acs.jpcc.1c09684](https://doi.org/10.1021/acs.jpcc.1c09684)

Publication date

2022

Document Version

Final published version

Published in

Journal of Physical Chemistry C

Citation (APA)

Van Veen, F. H., Ornago, L., Van Der Zant, H. S. J., & El Abbassi, M. (2022). Benchmark Study of Alkane Molecular Chains. *Journal of Physical Chemistry C*, 126(20), 8801-8806.
<https://doi.org/10.1021/acs.jpcc.1c09684>

Important note

To cite this publication, please use the final published version (if applicable).
Please check the document version above.

Copyright

Other than for strictly personal use, it is not permitted to download, forward or distribute the text or part of it, without the consent of the author(s) and/or copyright holder(s), unless the work is under an open content license such as Creative Commons.

Takedown policy

Please contact us and provide details if you believe this document breaches copyrights.
We will remove access to the work immediately and investigate your claim.

Benchmark Study of Alkane Molecular Chains

Frederik H. van Veen, Luca Ornago, Herre S. J. van der Zant,* and Maria El Abbassi*

Cite This: *J. Phys. Chem. C* 2022, 126, 8801–8806

Read Online

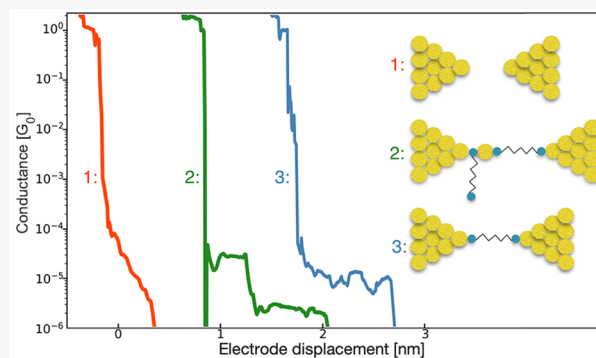
ACCESS |

Metrics & More

Article Recommendations

Supporting Information

ABSTRACT: Alkanes serve an important role as benchmark system in molecular electronics. However, a large variation in the conductance values is reported in the literature. To better understand these fluctuations, in this study we measure large molecular data sets (up to 100 000 breaking traces) of a series of alkanes with different lengths and anchoring groups using the mechanically controlled break junction (MCBJ) technique. Employing an unsupervised learning algorithm, we investigate both the time evolution and the distance dependence of the measured traces. For all the molecules considered, we have been able to identify the single-molecule conductance value for the fully stretched molecular configuration. For alkanedithiols, the corresponding extracted β decay constant of 1.05 ± 0.08 per CH_2 group agrees well with literature values. In the case of the stronger thiol bonding, additional peaks in the conductance histograms are found, suggesting the formation of molecular junctions containing a single molecule plus additional gold/molecule unit(s). The results shine light on the dispersion in reported conductance values and show that the evolution of the molecule as a function of stretching and time contains crucial information in determining the molecular junction configuration in MCBJs.



INTRODUCTION

Alkanes, simple saturated hydrocarbon chains, are one of the most studied molecules both in self-assembled monolayers (SAMs) and at the single-molecule scale. They serve as an important building block in a variety of applications within nanotechnology and chemistry. Alkanedithiols have, for example, been utilized for the integration of reproducible functional molecular compounds into solid-state devices,¹ the efficiency increase of (low-cost environmental-friendly) plastic solar cells,² and selectivity control of palladium catalysts.³ Because of their relatively easy synthesis, they are also among the most studied molecules in the field of single-molecule electronics, serving an important role as benchmark compounds, used for the calibration of different experimental and theoretical tools.⁴

Nevertheless, the electronic properties of the individual molecules and the molecular junction formation process are not yet well understood. For example, the single-molecule conductance is not well-defined, and a wide range of values have been reported by different groups for the same measurement technique. Different explanations, both structural and conformational, have been proposed to interpret these variations in the data, among which are gauche conformations in the molecular chain,^{5,6} different binding sites at the gold surface,⁵ chaining of additional units,^{7,8} and electrode shape differences.^{9,10} Understanding these fluctuations is crucial to increase the reliability and reproducibility in the different

applications. However, it remains challenging to experimentally demonstrate which of these explanations prevail.

In this study, we employ a new measurement/analysis strategy to address these issues by applying machine learning tools on a unique large conductance data set of a series of alkane molecules. We have employed an automated mechanically controlled break junction (MCBJ) setup and acquired uniquely large data sets of up to 100 000 consecutive breaking traces per sample. Traces cover a wide electrode displacement range for a series of alkane chains with different anchoring groups (Figure 1a). An unsupervised machine learning (ML) algorithm has been used to identify the conductance values belonging to the stretched single-molecule junction configuration.

EXPERIMENTAL SECTION

The device consists of a suspended gold nanowire on a flexible phosphor bronze substrate coated with an insulating layer of polyimide. By use of a three-point bending mechanism, comprising two counter supports and a pushing rod, the wire is stretched until it breaks, leaving two atomically sharp gold

Received: November 9, 2021

Revised: May 2, 2022

Published: May 17, 2022



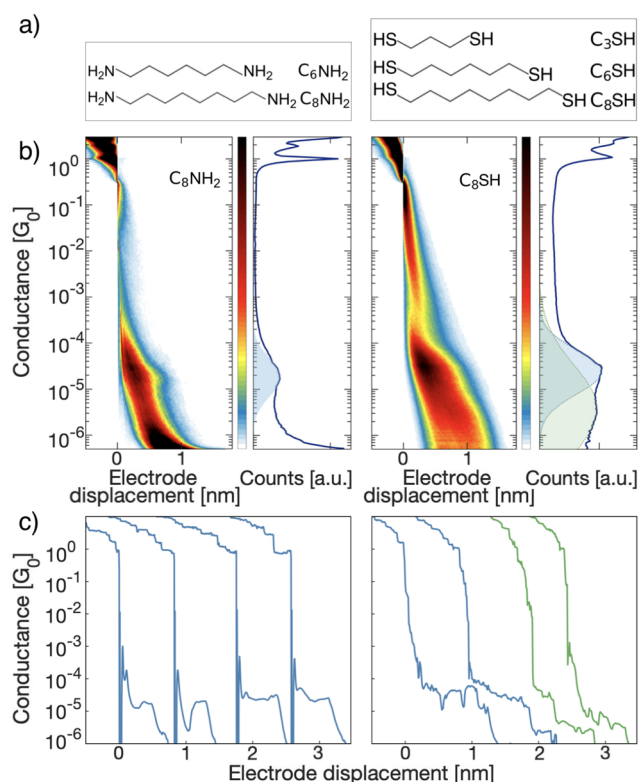


Figure 1. (a) Measured molecules: alkanes of different lengths (propane, hexane, and octane) with both thiol and amino anchoring groups. (b) Two-dimensional conductance vs electrode distance histogram, for octanediamine (left) and octanedithiol (right), constructed from 20 000 and 100 000 consecutive measurements, respectively. The shaded areas show the log-normal-distribution fits to prominent peaks. (c) Examples of individual breaking traces, offset horizontally, in the presence of octanediamine (left) and octanedithiol (right).

electrodes. Their separation can be modified with an accuracy of 10 pm by using a piezoelectric element. During a single breaking measurement, the separation is increased gradually, while the conductance of the associated junction is measured until it drops below the noise level, after which the wire is merged back together. One such event yields a single breaking trace, describing the conductance of the junction at different electrode displacements.

In the absence of molecules, the junction conductance decays exponentially as the gap between the electrodes increases, typical for tunneling across a barrier of increasing length. The molecular junction is formed when the target molecule bridges the gold electrodes, typically identified by the presence of a conductance plateau in the corresponding breaking trace. As electron transport through the molecular junction is sensitive to its geometry details, and by fluctuations of energy level alignment and electronic coupling, the conductance of the molecule is statistically determined by constructing conductance histograms from many breaking traces and fitting the prominent peak(s) with a log-normal distribution.

All the measurements in this study were conducted at room temperature, with a fixed applied bias voltage of 100 mV to ensure the formation stable junctions. Prior to molecular deposition, the bare gold sample is measured to both establish the cleanliness of the gold electrodes and to determine the

attenuation factor, describing the ratio between the vertical movement of the pushing rod and the horizontal displacement of the electrodes. A droplet of the target molecule solution is deposited only on the samples showing clean tunneling traces, and subsequent measurements are conducted.

An unsupervised clustering algorithm is then employed to separate the data set in classes of similar breaking traces. A detailed description of the clustering algorithm and clustering scheme can be found in the [Supporting Information](#) sections 1 and 2. For all plateaus appearing in the 2D histograms, the most probable conductance value is obtained from the log-normal fit to the corresponding peak in the 1D histograms. Additionally, the average lengths of the plateaus are computed, as described in the [Supporting Information](#) section 3. At room temperature the wire dissipates energy upon breaking, resulting in a stress-releasing snap-back of the freshly formed electrodes, with typically few counts between G_0 and $10^{-4}G_0$. To account for this snap-back effect, a length range of 0.3–0.6 nm¹¹ is added to the electrode displacements to estimate the junction length.

RESULTS

Figure 1b shows the 2D and 1D conductance histograms constructed from the raw data acquired for octanediamine (left) and octanedithiol (right). The shaded areas show the log-normal distribution fits to the prominent peaks. The raw data indicate an influence of the anchoring groups on the formed molecular junctions. For both molecules, a conductance peak is observed at roughly $2 \times 10^{-5}G_0$, highlighted by the blue shaded areas in the 1D histograms. For octanedithiol, however, an additional peak is observed at a lower conductance value, depicted by the additional green shaded area. The fits of this multimodal distribution were obtained by fitting the single peaks individually to visualize the presence of two peaks and determine the maximum conductance values. Typical individual traces corresponding to these peaks are shown in **Figure 1c**. For octanediamine, the traces display only plateaus at a conductance value similar to the single prominent peak in the 1D histogram. For octanedithiol, the blue and green traces display conductance plateaus at two distinct values, similar to those at which the equal-colored peaks in the corresponding 1D histogram are centered.

Figure 2 shows the results obtained from the unsupervised learning analysis of octanediamine. One molecular class is observed, labeled A, with a conductance plateau at $2.2 \times 10^{-5}G_0$ and an average plateau length of 0.6 nm. Accounting for the snap-back effect, an average junction length range of 0.9–1.2 nm is found, in good agreement with the estimated 1.13 nm length of a single fully stretched octanediamine molecule.¹² For all considered molecules, the plateau length histograms can be found in the [Supporting Information](#) section 4. Roughly 30% of the molecular traces display an initial exponential decay in conductance, followed by a jump to a conductance plateau. This behavior is well depicted in class A' of **Figure 2a** as well as **Figure 2b**, showing traces without (left) and with (right) a jump. The traces showing these jumps were not included in molecular class A. The complete set of octanediamine subclasses displaying such conductance jumps are shown in **Figure S6e**. The jumps occur at electrode displacements ranging from 0.3 to 0.5 nm, and the average conductance value after the jumps was found at $1.9 \times 10^{-5}G_0$, very similar to the conductance value obtained for class A. It is

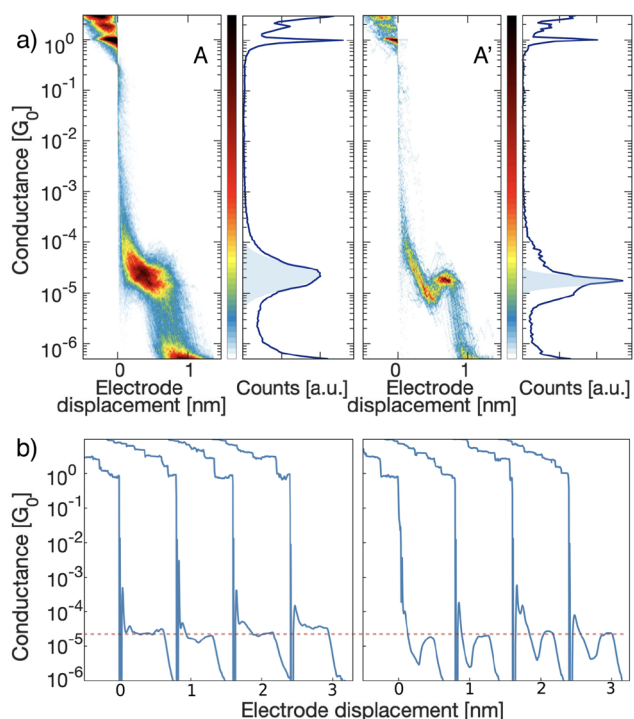


Figure 2. (a) Molecular classes observed after clustering analysis for octanediamine. The classes are labeled with the capital letter in the top-right corner of the two-dimensional conductance histograms. Class B is one of the subclasses that display traces with a jump in conductance, which were not included in class A. The corresponding one-dimensional conductance histograms are shown at the right side of the two-dimensional conductance histograms, with the shaded areas showing the log-normal-distribution fits to prominent peaks. (b) Examples of individual breaking traces for classes A (left) and A' (right), offset horizontally. A horizontal red dashed line is drawn at the most probable conductance value of class A.

important to note that this extracted conductance value is that of the peak corresponding to the plateau after the jump and not the most probable conductance value of the configuration during these breaking events. For hexanediamine, very similar behavior has been found (see [Supporting Information](#) section 4.1). One molecular class (A) is observed with a plateau at $1.1 \times 10^{-4} G_0$ and an average junction length range of 0.7–1.0 nm, which includes the estimated length of the fully stretched molecule (0.88 nm^{12}). As for octanediamine, a significant amount of the breaking traces display an initial exponential decaying conductance, followed by a jump to a plateau at an average $9.8 \times 10^{-5} G_0$, very similar to the conductance value obtained for class A. The hexanediamine subclasses displaying such conductance jumps are shown in [Figure S5](#).

For octanedithiol (a second data set comprising 100 000 traces consecutive breaking traces is presented in the [Supporting Information](#) section 4.5), three statistically significant classes (more than 3% of the traces) were obtained, which are shown in [Figure 3](#). Three additional classes (see [Supporting Information](#) section 4.5) were observed. The junctions corresponding to these classes, however, only start forming after the first 20 000 measurements, with the occurrence remaining low (below 3%) during the whole measurement. Class A (12% of the molecular traces) shows a plateau at $2.6 \times 10^{-5} G_0$, with an average plateau length of 0.4 nm. Class B (35% of the molecular traces) contains a plateau at

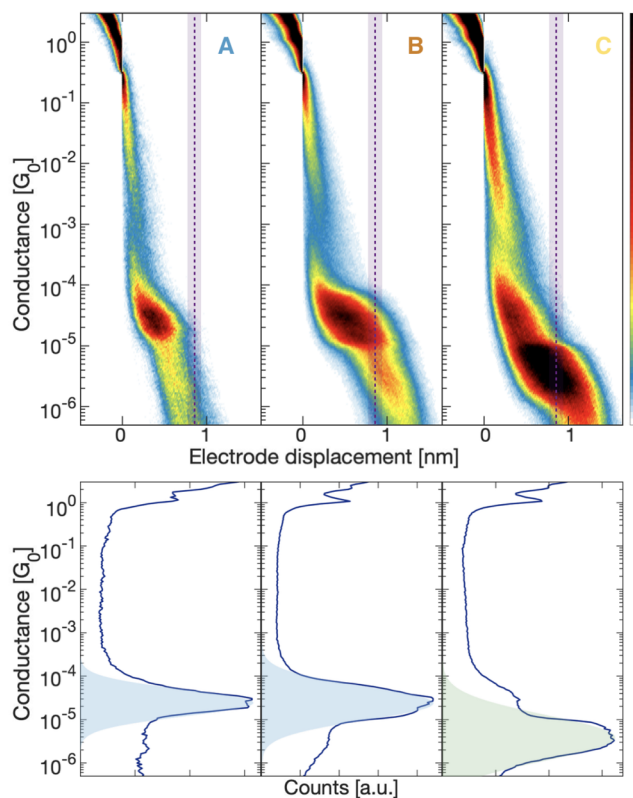


Figure 3. Molecular classes observed after the clustering analysis for octanedithiol. The corresponding one-dimensional conductance histograms are shown directly below the two-dimensional conductance histograms, with shaded areas showing the log-normal-distribution fits to the most prominent peaks. Purple dashed lines are drawn at the estimated single-molecule length (1.15 nm). The shaded purple areas around the dashed lines display a 10% error margin on this length.

a similar conductance value of $2.3 \times 10^{-5} G_0$. This plateau is however longer, with an average plateau length of 0.6 nm, and also less slanted than that of class A. Finally, class C (42% of the molecular traces) displays a double-step plateau, containing an initial shoulder at $2.2 \times 10^{-5} G_0$, very similar to the conductance of the single-step plateaus of classes A and B, followed by a prominent plateau at $3.6 \times 10^{-6} G_0$. The traces of this class exhibit on average a total length of 0.9 nm for the prominent conductance value and 0.3 nm for the shoulder. Both the length and conductance value of the shoulder of class C are very similar to the ones of class A. This may be an indication that class C initially forms a conformation similar to class A. Taking into account the snap-back effect, the final junction length ranges are 0.7–1.0 nm for class A, 0.9–1.2 nm for class B, and 1.2–1.5 nm for class C are found. Only traces from class B match the length of a fully stretched octanedithiol molecule at 1.15 nm.¹³ Class A subceeds this length while class C exceeds it. This is also depicted by the dashed purple lines in the 2D histograms drawn at the estimated single-molecule length.

The time evolution of the occurrence of the classes (i.e., the probability that a trace belonging to such class is measured) is presented in [Figure S13](#). A strong time dependence is observed for all the classes. Only class A is present in the first traces. A transition occurs after around 10 000 traces, and the yield of classes B and C increases with a very similar trend while traces

from class A become less probable. This trend is commonly observed in the case of thiol-protected molecules. Class A could correspond to a protected molecule, explaining the slanted plateau due to a weaker anchoring to the electrodes.¹⁴

The same clustering analysis was performed for the hexanedithiol, for which the obtained classes can be found in the Supporting Information section 4, and propanedithiol (to be discussed in the next paragraph; see Figure 4). For

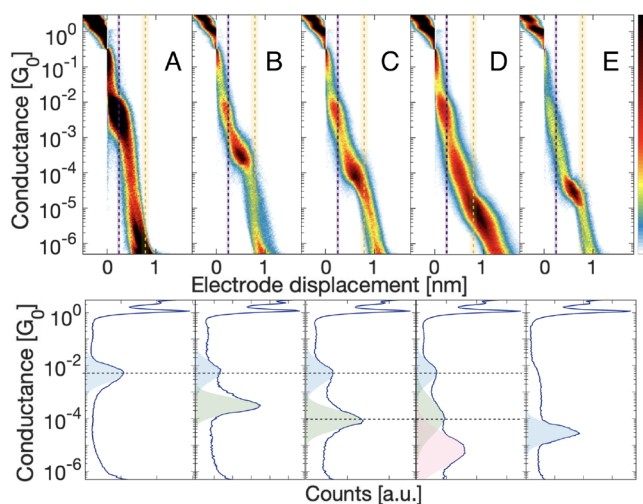


Figure 4. Molecular classes observed after the clustering analysis for propanedithiol. The corresponding one-dimensional conductance histograms are shown directly below the two-dimensional conductance histograms, with shaded areas showing the log-normal-distribution fits to the prominent peaks. Purple and yellow dashed lines are drawn at the estimated lengths of respectively one (0.53 nm) and two (1.06 nm) fully stretched propanedithiol molecules. The shaded areas around the dashed lines display a 10% error margin on this length. Horizontal dashed lines are drawn in the 1D conductance histograms to display the similarity between conductance values of peaks in different classes.

hexanedithiol, two classes with molecular features are obtained from the clustering analysis. Class A contains a plateau at $2.8 \times 10^{-4}G_0$, for which the corresponding average junction length is found within 0.8–1.1 nm, including the single-molecule length¹³ of 0.9 nm. Class B displays a plateau at a conductance value 10 times lower ($2.8 \times 10^{-5}G_0$). For the associated junctions, a length range of 1.0–1.3 nm is found, which exceeds the length of the fully stretched molecule significantly.

For propanedithiol, five distinct molecular classes are obtained upon clustering (see Figure 4). Classes A and E contain a single plateau, while multiple distinct plateaus are present for classes B (two), C (two), and D (three). The conductance values and final junction lengths are summarized in Table 1. All the classes display long traces except for class A, having a length comparable to the estimated single molecule length¹³ of 0.53 nm. This is further exemplified by the dashed purple and yellow lines in the 2D histograms, drawn at the lengths of one and two (consecutive) propanedithiol molecules, respectively. Three of these classes (B–D) contain distinct subsequent plateaus, which start at lengths greater than the single-molecule one, whereas the single plateau of class E also starts at a finite electrode displacement greater than the single-molecule length. For the multiple-plateau classes (B–D), we further observe a decay of the conductance as the final junction length increases. The initial plateaus of these classes

Table 1. Characteristics of the Plateaus Obtained for Propanedithiol

characteristic	class A	class B	class C	class D	class E
G top plateau	$4.7 \times 10^{-3}G_0$	$5.7 \times 10^{-3}G_0$	$3.6 \times 10^{-3}G_0$	$4.3 \times 10^{-3}G_0$	$2.9 \times 10^{-3}G_0$
G middle plateau		$4.3 \times 10^{-4}G_0$	$9 \times 10^{-5}G_0$	$1.1 \times 10^{-4}G_0$	
G bottom plateau				$6.3 \times 10^{-6}G_0$	
junction length (nm)	0.6–0.9	0.8–1.1	1.0–1.3	1.4–1.7	1.0–1.3

are all centered at a conductance value that is very similar to that of the single plateau of class A. This similarity, depicted by the top dashed horizontal line in the 1D histogram, suggests that configurations associated with classes B–D initially form the same configuration as the one associated with class A.

Classes B and C show very similar features. However, the merged class, as shown in Figure S8, displays two very subtle distinct peaks in the 1D histogram. For this reason, we consider them as two classes. Nevertheless, this is not changing the conclusion of our analysis, only excluding some of the possible conformations related to these classes proposed later in this study.

DISCUSSION

Alkanediamine molecules show only one molecular class displaying a clear single-step plateau. The average molecular junction lengths are estimated to lie within the size of the fully extended molecule. The conductance values of $1.1 \times 10^{-4}G_0$ (C6) and $2.2 \times 10^{-5}G_0$ (C8) correspond very well to the values found by Park et al.¹⁵ as well as the low-conductance values observed by Chen et al.¹⁶ The corresponding calculated β decay constant is 0.8 per CH_2 group (see Supporting Information section 4.6), in good agreement with the values reported in the literature: 0.81¹⁶ and 0.93¹⁷ per CH_2 group. Only in the case of alkanes with amino groups, resulting in a weaker binding to the electrodes, a significant amount of the molecular traces displays an initial exponentially decaying conductance followed by a jump upward to a conductance plateau, indicating a transition from background tunneling to molecular junction formation. The plateaus in this class are centered at a conductance value that is very similar to the identified single molecule one.

A larger variety of classes has been observed in the case of alkanedithiols. A class displaying a single-step plateau with an estimated range of junction length equaling the length of the corresponding fully stretched molecule has been observed for the three molecules (class B for octanedithiol and class A for both hexanedithiol and propanedithiol). These classes are attributed to the single-molecule junction formation. The plateaus for propanedithiol, octanedithiol, and hexanedithiol are centered at respectively $4.7 \times 10^{-3}G_0$, $2.8 \times 10^{-4}G_0$, and $2.3 \times 10^{-5}G_0$, in good agreement with the reported low-bias (100 mV) conductance values in the literature for propanedithiol,^{18,19} hexanedithiol,^{19–21} and octanedithiol.^{19,20,22}

From the identified single-molecule junction classes, the β decay constant is calculated to be 1.05 ± 0.08 per CH_2 group (see Supporting Information section 4.6). This value agrees well with the theoretically predicted values of 1²³ and 0.9²⁴ as well as $\beta_N = 0.9 \pm 0.2$, listed as the average value over many different experiments.⁴

For all alkanedithiols, classes with junction lengths exceeding that of a single fully stretched molecule, and additional peaks at conductance values lower than that of the identified single-molecule junctions, are observed. Several studies on alkanedithiols have reported the presence of multiple peaks, which were attributed to single-molecule junctions with different binding sites on the gold surface (i.e., top vs hollow)⁵ and the presence of gauche conformers.^{6,5} These effects are, however, unable to explain our longer configuration classes, even when disregarding junction lengths. Different binding arrangements predict conductance differences of at most a factor 4,⁵ while we observed conductance decreases of a factor 10. Gauche defects predict conductance differences of a factor 10,^{5,6,10} but the conductance was found to increase during junction elongation, as gauche defects are stretched out,^{6,10} whereas only decreases are observed in our case.

Except for propanedithiol class E, all of the longer-length classes display more than one plateau including the single-molecule one, suggesting configurations involving more than a single molecule. Several scenarios of junction formation are schematized in Figure 5a. Possible scenarios are visualized,

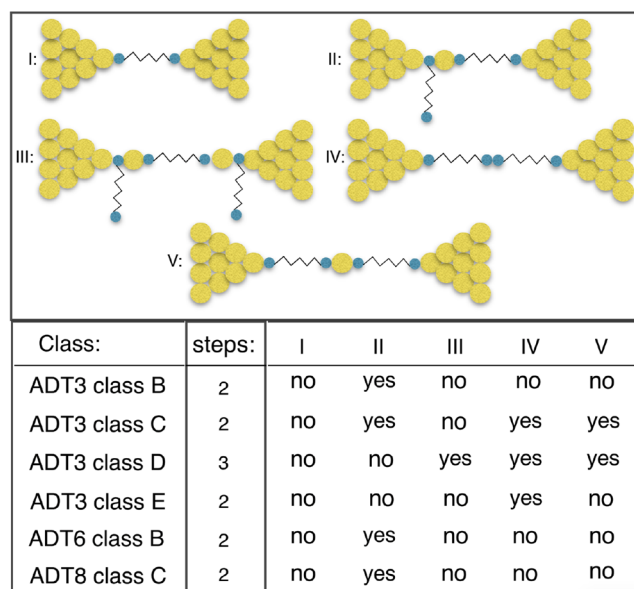


Figure 5. (a) Single-molecule junction configuration (I) and idealized configurations (II–V) yielding junction lengths exceeding the single-molecule length. (II) Formation of an additional gold–thiolate unit at one of the electrodes. (III) Formation of an additional gold–thiolate unit at both electrodes. (IV) Formation of a dimer chain, mediated by a disulfide bond. (V) Formation of a gold-linked dimer chain. (b) Amount of steps in the conductance histograms and summary of the scenario compatibilities, obtained from length increase and conductance decrease comparison, for the longer-length classes.

together with the single molecule junction (I). Chaining of an additional gold–thiolate unit at one (II) or two (III) electrode(s) has been reported,⁸ e.g., pentanedithiol in STM-BJ's, as well as the formation of gold-linked dimer and trimer chains (V), reported for 1,4-benzenediisocyanide molecules in the MCBJ setup.⁷ Finally, oligomerization could also occur via the spontaneous formation of disulfide bonds (IV), which has been observed for alkanedithiol molecules, organized in self-assembled monolayers.^{25,26} For all the classes with a total length larger than the one of a single molecule, agreements with the possible scenarios have been checked based on the

correspondences with the predicted length increase and conductance decay. This comparison serves as an initial exploration of the possible molecular conformations, already reported in the literature, that can explain the additional steps. Further analysis and theoretical support will be necessary to confirm any of the scenarios proposed. A more detailed explanation can be found in section 5 in the Supporting Information. The longer-configuration classes were compared to these scenarios, and the findings are together with the amount of steps in the conductance traces summarized in Figure 5b. The longer-configuration classes observed for hexanedithiol and octanedithiol are only compatible with scenario I, whereas dimer chains of these molecules are expected to result in conductance values below the noise level. For propanedithiol, it is more difficult to exclude any of the scenarios because the length increases and conductance decays of the different scenarios are quite similar for small chain lengths. Based on the length increase, class B is only consistent with scenario II, while conclusive answers lack for classes C and D. Finally, on the basis of the absence of the single-molecule plateau, we speculate that class E corresponds to dimerization via disulfide bonds. To further investigate the chaining dynamics experimentally, the hexanedithiols or octanedithiols should be measured in a setup with a lower noise level.

CONCLUSION

We have used an unsupervised clustering algorithm to investigate the junction configurations and corresponding conductance values of alkanedithiols (3,6 and 8 CH₂ groups) and alkanediamines (6 and 8 CH₂ groups) from large measurement sets, collected with an MCBJ setup. For all molecules, we identify classes corresponding to the single-molecule junction. From these, we extracted β decay constants of 1.05 ± 0.08 and 0.8 per CH₂ group for the alkanedithiols and alkanediamines, respectively, corresponding well with the literature. Differences in anchoring groups result in variations in the junction formation process. For weaker amino anchoring, several traces show a transition from background tunneling to a molecular plateau. While for stronger thiol binding, we observe additional classes containing lower conductance plateaus, which are attributed to thiol-mediated chaining of additional units: for octanedithiol and hexanedithiol our results strongly suggest the formation of additional gold–thiolate units at one of the electrodes. For propanedithiol, configurations containing gold-linked and disulfide-linked dimer chains of fully stretched molecules are also considered possible.

ASSOCIATED CONTENT

Supporting Information

The Supporting Information is available free of charge at <https://pubs.acs.org/doi/10.1021/acs.jpcc.1c09684>.

Figures S1–S17 and Tables S1–S7 (PDF)

AUTHOR INFORMATION

Corresponding Authors

Herre S. J. van der Zant – Kavli Institute of Nanoscience, Delft University of Technology, Delft 2628 CJ, The Netherlands; orcid.org/0000-0002-5385-0282; Email: H.S.J.vanderZant@tudelft.nl

Maria El Abbassi – Kavli Institute of Nanoscience, Delft University of Technology, Delft 2628 CJ, The Netherlands; orcid.org/0000-0001-5177-6528; Email: M.ElAbbassi-1@tudelft.nl

Authors

Frederik H. van Veen – Kavli Institute of Nanoscience, Delft University of Technology, Delft 2628 CJ, The Netherlands
Luca Ornago – Kavli Institute of Nanoscience, Delft University of Technology, Delft 2628 CJ, The Netherlands

Complete contact information is available at:
<https://pubs.acs.org/10.1021/acs.jpcc.1c09684>

Notes

The authors declare no competing financial interest.

ACKNOWLEDGMENTS

This study was partially funded by the FET open project QuIET (no. 767187). The device fabrication was done at the Kavli Nanolab at Delft. The authors gratefully thank R. Wasserman for his preliminary analysis and M. and Y. Abbad Andaloussi for proofreading the paper.

REFERENCES

- (1) Puebla-Hellmann, G.; Venkatesan, K.; Mayor, M.; Lortscher, E. Metallic nanoparticle contacts for high-yield, ambient-stable molecular-monolayer devices. *Nature* **2018**, *559*, 232–235.
- (2) Peet, J.; Kim, J. Y.; Coates, N. E.; Ma, W. L.; Moses, D.; Heeger, A. J.; Bazan, G. C. Efficiency enhancement in low-bandgap polymer solar cells by processing with alkane dithiols. *Nat. Mater.* **2007**, *6*, 497–500.
- (3) Marshall, S. T.; O'Brien, M.; Oetter, B.; Corpuz, A.; Richards, R. M.; Schwartz, D. K.; Medlin, J. W. Controlled selectivity for palladium catalysts using self-assembled monolayers. *Nat. Mater.* **2010**, *9*, 853–858.
- (4) Evers, F.; Korytár, R.; Tewari, S.; van Ruitenbeek, J. M. Advances and challenges in single-molecule electron transport. *Rev. Mod. Phys.* **2020**, *92*, 035001.
- (5) Li, C.; Pobelov, I.; Wandlowski, T.; Bagrets, A.; Arnold, A.; Evers, F. Charge Transport in Single Au — Alkanedithiol — Au Junctions: Coordination Geometries and Conformational Degrees of Freedom. *J. Am. Chem. Soc.* **2008**, *130*, 318–326.
- (6) Paulsson, M.; Krag, C.; Frederiksen, T.; Brandbyge, M. Conductance of Alkanedithiol Single-Molecule Junctions: A Molecular Dynamics Study. *Nano Lett.* **2009**, *9*, 117–121.
- (7) Vladyka, A.; Perrin, M.; Overbeck, J.; Ferradás, R.; García-Suárez, V.; Gantenbein, M.; Brunner, J.; Mayor, M.; Ferrer, J.; Calame, M. In-situ formation of one-dimensional coordination polymers in molecular junctions. *Nat. Commun.* **2019**, *10*, 262.
- (8) Leary, E.; Zotti, L. A.; Miguel, D.; Márquez, I. R.; Palomino-Ruiz, L.; Cuerva, J. M.; Rubio-Bollinger, G.; González, M. T.; Agrait, N. The Role of Oligomeric Gold–Thiolate Units in Single-Molecule Junctions of Thiol-Anchored Molecules. *J. Phys. Chem. C* **2018**, *122*, 3211–3218.
- (9) Perrin, M. L.; Verzijl, C. J. O.; Martin, C. A.; Shaikh, A. J.; Eelkema, R.; van Esch, J. H.; van Ruitenbeek, J. M.; Thijssen, J. M.; van der Zant, H. S. J.; Dulić, D. Large tunable image-charge effects in single-molecule junctions. *Nat. Nanotechnol.* **2013**, *8*, 282–287.
- (10) Li, Z.; Mejía, L.; Marrs, J.; Jeong, H.; Hihath, J.; Franco, I. Understanding the Conductance Dispersion of Single-Molecule Junctions. *J. Phys. Chem. C* **2021**, *125*, 3406–3414.
- (11) Huang, C.; Rudnev, A. V.; Hong, W.; Wandlowski, T. Break junction under electrochemical gating: testbed for single-molecule electronics. *Chem. Soc. Rev.* **2015**, *44*, 889–901.
- (12) McNeely, J.; Miller, N.; Pan, X.; Lawson, B.; Kamenetska, M. Angstrom-Scale Ruler Using Single Molecule Conductance Signatures. *J. Phys. Chem. C* **2020**, *124*, 13427–13433.
- (13) Sek, S.; Misicka, A.; Swiatek, K.; Maicka, E. Conductance of -Helical Peptides Trapped within Molecular Junctions. *J. Phys. Chem. B* **2006**, *110*, 19671–19677.
- (14) El Abbassi, M.; Zwick, P.; Rates, A.; Stefani, D.; Prescimone, A.; Mayor, M.; van der Zant, H. S. J.; Dulić, D. Unravelling the conductance path through single-porphyrin junctions. *Chemical Science* **2019**, *10*, 8299–8305.
- (15) Park, Y. S.; Whalley, A. C.; Kamenetska, M.; Steigerwald, M. L.; Hybertsen, M. S.; Nuckolls, C.; Venkataraman, L. Contact Chemistry and Single-Molecule Conductance: A Comparison of Phosphines, Methyl Sulfides, and Amines. *J. Am. Chem. Soc.* **2007**, *129*, 15768–15769.
- (16) Chen, F.; Li, X.; Hihath, J.; Huang, Z.; Tao, N. Effect of Anchoring Groups on Single-Molecule Conductance: Comparative Study of Thiol-, Amine-, and Carboxylic-Acid-Terminated Molecules. *J. Am. Chem. Soc.* **2006**, *128*, 15874–15881.
- (17) Venkataraman, L.; Klare, J. E.; Tam, I. W.; Nuckolls, C.; Hybertsen, M. S.; Steigerwald, M. L. Single-Molecule Circuits with Well-Defined Molecular Conductance. *Nano Lett.* **2006**, *6*, 458–462.
- (18) Hihath, J.; Arroyo, C. R.; Rubio-Bollinger, G.; Tao, N.; Agrait, N. Study of Electron-Phonon Interactions in a Single Molecule Covalently Connected to Two Electrodes. *Nano Lett.* **2008**, *8*, 1673–1678.
- (19) Arroyo, C. R.; Leary, E.; Castellanos-Gómez, A.; Rubio-Bollinger, G.; González, M. T.; Agrait, N. Influence of Binding Groups on Molecular Junction Formation. *J. Am. Chem. Soc.* **2011**, *133*, 14313–14319.
- (20) Jang, S.-Y.; Reddy, P.; Majumdar, A.; Segalman, R. A. Interpretation of Stochastic Events in Single Molecule Conductance Measurements. *Nano Lett.* **2006**, *6*, 2362–2367.
- (21) Ulrich, J.; Esrail, D.; Pontius, W.; Venkataraman, L.; Millar, D.; Doerrer, L. H. Variability of Conductance in Molecular Junctions. *J. Phys. Chem. B* **2006**, *110*, 2462–2466.
- (22) Cui, X. D.; Primak, A.; Zarate, X.; Tomfohr, J.; Sankey, O. F.; Moore, A. L.; Moore, T. A.; Gust, D.; Harris, G.; Lindsay, S. M. Reproducible Measurement of Single-Molecule Conductivity. *Science* **2001**, *294*, 571–574.
- (23) Tomfohr, J.; Sankey, O. F. Theoretical analysis of electron transport through organic molecules. *J. Chem. Phys.* **2004**, *120*, 1542–1554.
- (24) Picaud, F.; Smogunov, A.; Corso, A.; Tosatti, E. Complex band structures and decay length in polyethylene chains. *J. Phys.: Condens. Matter* **2003**, *15*, 3731–3740.
- (25) Millone, M. A. D.; Hamoudi, H.; Rodríguez, L.; Rubert, A.; Benítez, G. A.; Vela, M. E.; Salvarezza, R. C.; Gayone, J. E.; Sánchez, E. A.; Grizzi, O.; Dablemont, C.; Esaulov, V. A. Self-Assembly of Alkanedithiols on Au(111) from Solution: Effect of Chain Length and Self-Assembly Conditions. *Langmuir* **2009**, *25*, 12945–12953.
- (26) Kohli, P.; Taylor, K. K.; Harris, J. J.; Blanchard, G. J. Assembly of Covalently-Coupled Disulfide Multilayers on Gold. *J. Am. Chem. Soc.* **1998**, *120*, 11962–11968.